Hydrogeology Journal (2021) 29:687–701
https://doi.org/10.1007/s10040-020-02256-1

PAPER

Geochemical insights into groundwater movement in alpine karst, Bear River Range, Utah, USA

Thomas Lachmar[1] · Skyler Sorsby[2] · Dennis Newell[1]

Received: 6 June 2020 / Accepted: 9 October 2020 / Published online: 17 October 2020

Abstract

Alpine karst aquifers control the availability and longevity of some water resources, but are not well understood. A conceptual model of the alpine karst aquifer system in the Bear River Range of northern Utah (USA) has been developed by geochemical analysis (major ions, $\delta^{18}O$, $\delta^{2}H$ and $\delta^{13}C$ values) of seasonal water samples from seven perennial springs, and residence-time assessment (^{3}H and CFCs) of two low- and two high-discharge springs. All spring data can be explained by reaction paths dominated by the dissolution of calcian dolomite. The $\delta^{13}C$ values align well with reaction paths for open-system dissolution. Saturation indices and low Ca:Mg molar ratios indicate that incongruent dissolution exerts a strong control on water–rock interactions, complicating interpretation of natural solute tracers. Values of $\delta^{18}O$ and $\delta^{2}H$ in springs follow the Utah meteoric water line. Snow $\delta^{18}O$ values correlate with elevation, but not with increasing rainout distance, providing qualitative estimates of recharge elevation that generally align with previous dye-traces to five of the seven springs. Concentrations of ^{3}H and CFCs likely are best described by binary mixing of subannual recharge with 60–65-year-old groundwater, suggesting that the alpine karst aquifer system in the Bear River Range is best represented by a double-porosity model. Subannual recharge documented by dye traces implies that caverns are the primary flowpaths to the springs, but the presence of decadal-age water may indicate that lower permeability flowpaths dominate during baseflow. No evidence was found for a longer-residing flow component, suggesting high sensitivity to future climate variability.

Keywords Carbonate rocks · Hydrochemical modeling · Stable isotopes · Groundwater age · USA

Introduction

Approximately 25% of the Earth's population relies on karst-hosted groundwater (Ford and Williams 2007). In mountainous regions with extensive carbonate bedrock, "alpine karst aquifers" host the majority of groundwater, and are sensitive to changing recharge and precipitation patterns due to climate change (Ozyurt 2008; Moral et al. 2008; Goldscheider and Neukum 2010; Zeng et al. 2012; Frondini et al. 2014)—for example, approximately 50% of the population of Austria, including its capital, Vienna, relies on water from such aquifers (Savio et al. 2019). However, because of difficult accessibility, alpine karst aquifers have received little attention, and almost exclusively in the Alps (Chen and Goldscheider 2014; Filippini et al. 2018; Gremaud et al. 2009; Lauber and Goldscheider 2014). In fact, the only studies of alpine karst in North America were conducted in the Canadian Rocky Mountains in the 1980s (Ford 1983; Smart 1983, 1988). Furthermore, no studies of such aquifers have been conducted in arid to semiarid regions, such as the western United States, where water supplies in these aquifers may be adversely impacted by the effects of climate change. The Bear River Mountains of northern Utah are an excellent field laboratory to improve the understanding of groundwater recharge and movement in alpine karst aquifers.

The north–south trending Bear River Range in northern Utah is located in the Rocky Mountain province of the western United States, bounded on the west by Cache Valley that hosts the city of Logan and other communities (Fig. 1). It contains an alpine karst aquifer system that sustains the baseflow of the Logan River (Gooseff et al. 2005; Kolesar et al. 2005), the largest stream in the range. A number of springs drain into the

✉ Thomas Lachmar
tom.lachmar@gmail.com

[1] Department of Geosciences, Utah State University, 4505 Old Main Hill, Logan, UT 84322, USA

[2] Golder Associates Inc., 200 Century Parkway, Suite C, Mt. Laurel, NJ 08054, USA

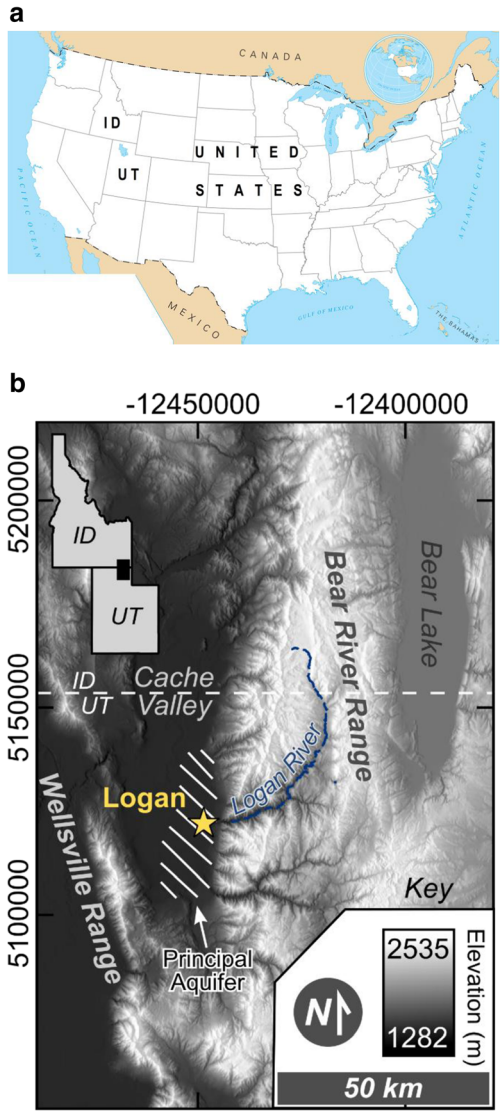

Fig. 1 **a** Location of the study area in the USA. **b** Topography of Cache Valley and the Bear River Range in northern Utah (UT) and southern Idaho (ID). The principal aquifer is shown as small white lines. The coordinate system is UTM Zone 12 N

Logan River, one of which, Dewitt Spring, is the primary source of water for the city of Logan (Spangler 2001), the largest city in Cache Valley. The eastern margin of Cache Valley hosts a highly productive aquifer system (Bjorklund and McGreevy 1971), later termed the principal aquifer by Robinson (1999), that is recharged in part by the Logan River.

Nearly 7,600 m of Paleozoic marine limestones, dolostones and interbedded siliciclastic deposits comprise the bedrock geology of the Bear River Range (Williams 1948, 1958; Francis 1972). Quartzites and shales separate thick carbonate aquifer units and likely act as aquicludes (Dover 1995). The East Cache fault, a Basin-and-Range normal fault, cuts the west limb of the NNE-trending, south-plunging, Sevier-age Logan Peak syncline (Williams 1948; McCalpin 1989, 1994; Evans and Oaks 1996; Evans et al. 1996). The syncline (Fig. 2) funnels groundwater flow south to seven primary springs draining limestone- and dolostone-aquifer units adjacent to the Logan River (Fig. 2). The spring discharges range from 0.03 to 0.71 m^3/s (Mundorff 1971; Spangler 2001).

Dissolution of carbonate minerals can enhance the permeability of fractures, bedding planes and pore space in karst aquifers, with most flow typically occurring in solution-enhanced conduits and most storage occurring interstitially if enhanced pore space is present (White 2003). The resulting flowpath architecture may adhere to one of three conceptual karst flow models (Fig. 3): (*flowpath a*) a single-porosity model assumes that all groundwater moves through conduits on the order of days to weeks; (*flowpath b*) a double-porosity model adds an intermediate velocity component (years to decades) that moves along less-enhanced fractures; and (*flowpath c*) a triple-porosity model adds a third component of slow velocity (hundreds to thousands of years) that moves through solution-enhanced pore space.

Dye traces in the Bear River Range indicate that groundwater flow along bedding planes and solution-enhanced fractures can cross topographic divides and drop up to 300 m, spending as little as 2–4 weeks in the subsurface (Spangler 2001, 2012; Bahr 2016). Bright (2009) used tritium data to identify possible decadal residence times for springs in the eastern Bear River Range. This bimodal age distribution aligns with that observed in a low-relief karst aquifer in Florida (Katz et al. 2009). Kolesar et al. (2005) and Neilson et al. (2018) both inferred the possibility for zones of slow karst development based on major-ion data of the Logan River and major tributary springs. Whereas matrix-dominated flowpaths of this type are documented in low-relief karst aquifers, geochemical lines of evidence used in alpine systems rarely address natural processes or anthropogenic solutes that confound interpretation. The presence or absence of groundwater with long (centennial to millennial) residence times has significant implications for water resource sensitivity to a variable climate.

The purposes of this study are to develop a conceptual model of the alpine karst aquifer system in the Bear River Range, and to increase the understanding of alpine karst aquifers in general by quantifying water–rock interactions and residence times. The new data reported here include major ion chemistry, oxygen and hydrogen stable isotope ratios ($\delta^{18}O$ and $\delta^{2}H$ values), stable isotope ratios of dissolved inorganic carbon ($\delta^{13}C$ values), and tritium (^{3}H) and chlorofluorocarbon (CFC) concentrations from the seven springs, as well as the $\delta^{18}O$ of snow cores from 17 locations. These data are used to: (1) determine if springs have geochemical signatures that relate to specific hydrogeologic flowpaths, and if average spring discharge magnitudes indicate open-system (high discharge) or closed-system (low discharge) dissolution of calcite and dolomite; (2) calculate carbonate mineral saturation indices to ascertain whether geochemical signatures are controlled

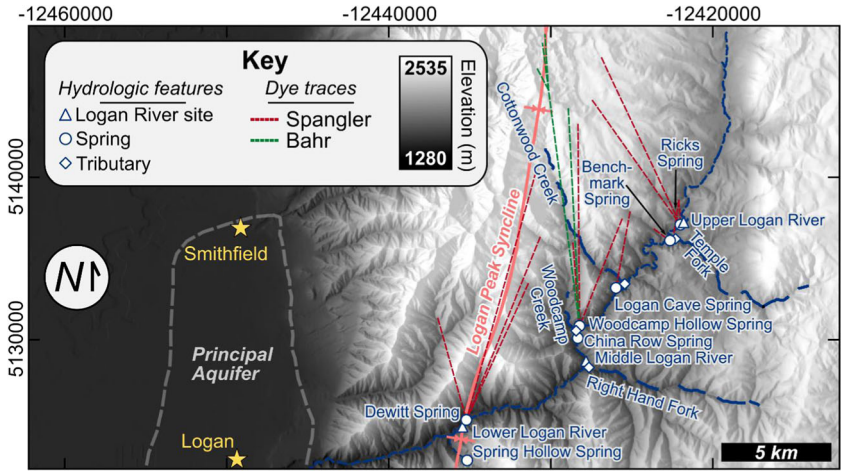

Fig. 2 Location of the Logan Peak syncline, and springs, streams and dye traces in Logan Canyon, Bear River Range (Spangler 2001; Bahr 2016)

by dissolution processes or instead impart flowpath-specific fingerprints; (3) assess whether springs drain groundwater in equilibrium with contemporary atmospheric values reflective of short (weeks to months) or indicate longer (decadal or older) residence times; and (4) determine if snowpack isotopic values can be used to estimate groundwater recharge elevation for these springs. The data reported here were collected in March, May and November of 2017.

Materials and methods

Field chemical parameters

Temperature, pH, electrical conductivity (EC), dissolved oxygen (DO) and carbonate alkalinity were measured in the field at all seven springs during all three chemical sampling excursions. A YSI-30 m was used to measure temperature and EC during the first two excursions, but was replaced by a YSI EcoSense EC 300A meter for the third excursion. An Orion 2013A pH meter, a Hanna HI 9142 dissolved-oxygen meter, and a Hach model AL-AP MG-L alkalinity test kit were used to measure pH, DO and alkalinity, respectively, during all three field excursions. Total alkalinity also was measured by laboratory colorimetric titration to reduce error (±0.05 mg/L as HCO_3) over the Hach field test kit (±20 mg/L as HCO_3). Only the results from the laboratory titrations are reported here.

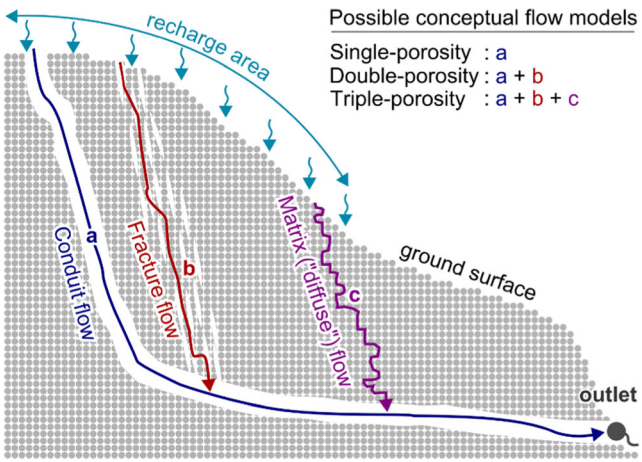

Fig. 3 Schematic of single, double and triple porosity conceptual models (after White 2003). Subsurface white areas are void space

Major ion analysis

Samples for major ion analysis were collected from each spring during low-flow (4 March 2017) and high-flow (31 May 2017) conditions. Samples were collected in November 2017 only at Benchmark, China Row, Spring Hollow (2 November) and Dewitt (3 November) Springs. Chemically clean polyethylene bottles were prerinsed, filled with filtered (0.45 μm) sample water, and acidified with 1:1 trace-metal-grade nitric acid to a pH less than 2 (Wilde 2008). Samples for anion (chloride and sulfate) analysis were collected in glass bottles without acidification or filtering. All samples were refrigerated prior to analysis. Cation and anion analyses were performed at Utah State University (USU) Geochemistry Lab and the USU Water Research Lab using a Thermo X Series 2 Quadrupole inductively-coupled plasma mass spectrometer (ICP-MS) and a Dionex ion chromatograph (IC) to ±0.1 and 1.1 mg/L accuracy, respectively. The unacidified, unfiltered samples were also titrated for alkalinity as bicarbonate with 0.02 N sulfuric acid and Bromo Blue indicator to ±0.05 mg/L accuracy at the USU Geochemistry Lab.

O, H and C stable isotope ratios

Samples for O and H stable-isotope analysis were collected on 4 March and 31 May 2017 in chemically clean, clear glass bottles and refrigerated prior to analysis. Samples for C stable-isotope analysis were collected at the same time and in the same manner as O and H samples, but in amber glass bottles

with no headspace to minimize aquatic biological-fractionation due to microbial activity (Mook 2001).

Snow samples for O and H stable isotopes were collected in March 2017 with a custom 10-ft (3.05 m) PVC toothed snow coring tool. The tool was driven through the snowpack until the soil was reached. The core then was cleaned of soil, ejected into a 1-gal plastic bag until melted, transferred to a chemically clean, clear glass bottle and refrigerated until analysis. Cores were collected over a range of elevations (1,543–2,393 m asl) where the snowpack was pristine and unaltered by remobilization via wind or anthropogenic activity.

Analyses for O, H and C stable isotope ratios were performed at the USU Stable Isotope Lab using a Thermo Scientific Delta V Advantage isotope-ratio mass spectrometer (IRMS) with a Gasbench II peripheral. The stable-isotope values were corrected for temporal drift and linearity effects as appropriate using in-house standards and calibrated to international standards and are reported using delta notation in per mille (‰). The $\delta^{18}O$ and $\delta^{2}H$ values of water and snow are reported $\pm$0.06 and 2.0‰, respectively, versus Vienna Standard Mean Ocean Water (VSMOW). The $\delta^{13}C$ values of dissolved inorganic carbon (DIC) are reported $\pm$0.1‰ versus Vienna Pee Dee Belemnite (VPDB). To quantify the statistical relationship of $\delta^{18}O$ values to elevation and location ("rainout" distance), bulk-snowpack stable-isotope values were assessed with analysis-of-variance. Linear regression was used to estimate a local elevation gradient, in ‰ per 100 m, after James et al. (2000). Precision for a data-dense $\delta^{18}O$ elevation gradient is on the order of ±0.5‰ (Brooks et al. 2012).

Tritium and chlorofluorocarbon sampling and analyses

Two low-discharge springs (Benchmark, China Row) and two high-discharge springs (Dewitt, Spring Hollow) on either side of the Logan River were sampled for ^{3}H and CFCs on 2 November (Benchmark, China Row and Spring Hollow) and 3 November (Dewitt) 2017. Tritium samples were collected in chemically clean 1-L Nalgene bottles such that no bubbles remained after pre-rinsing with spring water (Solomon 2017). Samples were transported overnight to Brigham Young University (BYU) and analyzed to a precision of ±0.1 TU and a detection limit of 0.3 TU using a Quantulus ultra-low-level liquid-scintillation counter after electrolytic enrichment (S. Nelson, Brigham Young University, written communication, 2017).

Chlorofluorocarbon samples were collected in accordance with USGS GDL (2017), using a peristaltic pump with Viton and copper tubing extended to the base of a 4-oz Boston-type glass bottle within a 1-gal stainless-steel container. The container was allowed to overflow such that a minimum of one gallon flushed through the sample bottle. The bottle then was capped (foil-lined) underwater with no visible air bubbles, inverted, and stored at room temperature until delivery to the University of Utah Dissolved and Noble Gas Lab the next day. The samples were analyzed to a precision of ±5%, and a detection limit of 1 pg/kg for CFC-113 and 0.5 pg/kg for CFC-11 and CFC-12.

Geochemical modeling

Reaction paths for water-chemistry evolution were created with the PHREEQC geochemical model using the *llnl* database (Parkhurst and Appelo 2013; after Langmuir 1971). The enthalpies of reaction for dissolution of stoichiometric calcite and stoichiometric dolomite were obtained from the PHREEQC *llnl* database. The enthalpy of reaction for dissolution of magnesian calcite was selected from Bischoff (1998). The enthalpy of reaction for dissolution of calcian dolomite was set to a default value of zero, which is standard in the absence of a thermodynamic estimate.

These models simulate simple end-member conditions for equilibrium water–rock–CO_2 interactions in open- or closed-systems. Equilibrium speciation, mineral saturation indices and pCO_2 were calculated for equilibration with dolomite or calcite to assess similarity of the models to field data. Carbon mass-balance modeling after Frondini et al. (2014) was performed using $\delta^{13}C$ as a response variable to distinguish more readily open- and closed-system dissolution.

Lumped parameter modeling

Tracers such as ^{3}H and CFCs are used to estimate groundwater ages by lumped-parameter modeling (Solder et al. 2016). The standard suite of lumped-parameter models, TracerLPM, is maintained by the US Geological Survey (USGS). Choosing the best model requires an understanding of the input functions for atmospheric concentrations of each tracer.

Tritium atmospheric concentrations were monitored at the IAEA Ottawa, Canada station until 2012 (IAEA 2014), after which records were extended with the known decay rate. It is the most complete atmospheric record in North America, and is commonly correlated with incomplete records at other locations to estimate the local atmospheric history (Michel 1989). The ^{3}H record for Ottawa was correlated with the incomplete record from Salt Lake City (1963–1984) to produce a local estimate of atmospheric concentrations of ^{3}H. Chlorofluorocarbon atmospheric concentrations are documented historically, and currently monitored at the Niwot Ridge facility in Colorado (Niwot Ridge LTER 2018).

Results

Field chemical parameters

Water with the lowest temperatures emerged from Dewitt and Spring Hollow springs (6.4 °C) in May and March, respectively, and the warmest water emerged from Benchmark Spring (11.0 °C) in May. All springs are near neutral, with pH values ranging from 7.1 to 7.8. Electrical conductivities ranged from 193 μS/cm at Woodcamp Hollow Spring in March to 446 μS/cm at China Row Spring in November. Dissolved-oxygen concentrations are relatively invariant across space and time, although concentrations in large springs (10.3–11.6 mg/L) exceeded concentrations in Benchmark and China Row Springs (5.4–8.8 mg/L). Alkalinity via laboratory colorimetric titration ranged from 208 and 305 mg/L (Table 1).

Major ion concentrations

Major-ion concentrations are summarized in Table 1. Major ions are dominated by Ca^{2+}, Mg^{2+} and HCO_3^- across seasons. Anomalously high levels of Na^+ and Cl^- are present in China Row Spring in March and May, but were similar to other springs when resampled in November. Concentrations in the original two samples likely reflect contamination by road salt used during the winter months. These anomalous Na^+ and Cl^- results do not adversely impact interpretations presented in this paper.

Mineral saturation index and pCO_2 calculations in PHREEQC

Mineral saturate states were determined using PHREEQC and are reported as the saturation index (SI):

$$SI = [\text{ion activity product}] \div K_{sp} \quad (1)$$

where K_{sp} is the solubility product (Table 2). Langmuir (1971) estimated equilibrium with respect to calcite and dolomite to be ±0.1 SI units (SI = 0 indicates equilibrium saturation), but propagation of error in this study (pH = ±0.1, Ca^{2+} and Mg^{2+} = ±1 mg/L) indicates that a value of ±0.3 is more appropriate. Saturation indices with respect to stoichiometric calcite and stoichiometric dolomite range from undersaturated to saturated and saturated to supersaturated, respectively. However, Spring Hollow Spring was undersaturated with respect to both calcite and dolomite in March. Carbon dioxide log partial pressures are shown in Table 2. Logan Cave and China Row Springs exhibit the highest partial pressures (log pCO_2 = −2.1 atm). Benchmark and Woodcamp Hollow Springs exhibit the lowest (−2.5 atm).

Table 1 Major ions in springs from all chemical sampling excursions (all units in mg/L)

Spring	Date	Ca^{2+}	Mg^{2+}	Na^+	K^+	HCO_3^-	SO_4^{2-}	Cl^-
Ricks	3/4/2017	37.8	19.8	5.6	1.5	234	2.2	18.2
Benchmark	3/4/2017	38.4	22.4	5.0	1.8	250	3.0	7.3
Logan Cave	3/4/2017	33.9	22.2	2.1	1.6	238	3.1	7.3
Woodcamp	3/4/2017	32.4	26.8	1.3	1.1	242	2.1	1.4
China Row[a]	3/4/2017	44.0	28.6	30.7	1.6	283	4.8	55.2
Dewitt	3/4/2017	36.2	22.7	3.4	1.6	256	7.4	3.9
Spring Hollow	3/4/2017	38.1	19.6	3.5	1.6	224	14.8	2.0
Ricks	5/31/2017	37.8	17.0	1.6	1.7	238	1.2	1.3
Benchmark	5/31/2017	28.3	16.6	3.9	1.7	262	2.2	1.8
Logan Cave	5/31/2017	32.0	19.5	1.6	1.5	226	3.2	6.5
Woodcamp	5/31/2017	26.6	23.3	0.6	0.3	226	0.8	0.6
China Row[a]	5/31/2017	39.6	26.8	23.8	0.5	305	4.7	31.7
Dewitt	5/31/2017	33.8	12.9	1.3	1.3	208	3.0	1.2
Spring Hollow	5/31/2017	40.8	12.6	1.8	1.8	232	3.9	1.8
Benchmark	11/2/2017	49.4	16.8	4.3	0.7	250	3.2	6.7
China Row	11/2/2017	55.6	19.6	7.4	0.9	287	4.0	7.3
Dewitt	11/3/2017	44.3	15.2	1.3	0.8	232	7.8	1.2
Spring Hollow	11/2/2017	50.9	15.0	2.2	2.5	232	16.3	2.2

[a] Na^+ and Cl^- concentrations impacted by road salt contamination

Table 2 Calculated log pCO_2 and saturation indices (SI) for stoichiometric calcite and dolomite, and calcian dolomite

Spring	Date	Log pCO_2	SI Stoichiometric Calcite	SI Stoichiometric Dolomite	SI Calcian Dolomite
Ricks	3/4/2017	−2.2	−0.4	0.2	−0.9
Benchmark	3/4/2017	−2.5	0.0	1.2	0.1
Logan Cave	3/4/2017	−2.1	−0.5	0.1	−0.9
Woodcamp	3/4/2017	−2.5	0.0	1.2	0.1
China Row	3/4/2017	−2.1	−0.3	0.5	−0.5
Dewitt	3/4/2017	−2.3	−0.2	0.6	−0.5
Spring Hollow	3/4/2017	−2.0	−0.7	−0.5	−1.5
Ricks	5/31/2017	−2.2	−0.3	0.4	−0.7
Benchmark	5/31/2017	−2.2	−0.2	0.6	−0.5
Logan Cave	5/31/2017	−2.3	−0.4	0.4	−0.7
Woodcamp	5/31/2017	−2.4	−0.3	0.6	−0.5
China Row	5/31/2017	−2.1	−0.2	0.7	−0.4
Dewitt	5/31/2017	−2.4	−0.2	0.4	−0.6
Spring Hollow	5/31/2017	−2.3	−0.2	0.3	−0.7
Benchmark	11/2/2017	−2.2	−0.1	0.6	−0.5
China Row	11/2/2017	−2.2	0.0	0.8	−0.3
Dewitt	11/3/2017	−2.4	−0.1	0.6	−0.4
Spring Hollow	11/2/2017	−2.4	−0.1	0.6	−0.4

Stable isotope ratios

The $\delta^{18}O$, $\delta^{2}H$ and $\delta^{13}C$ (DIC) values for spring waters are reported in Table 3. The $\delta^{18}O$ values for springs in 2017 range from −18.2 to −16.5‰ during high- and low-flow conditions, respectively. Corresponding spring $\delta^{2}H$ values range from −135‰ during high-flow conditions up to −124‰ during low-flow conditions. The $\delta^{18}O$ and $\delta^{2}H$ values of snow core samples collected in March 2017 (Table 4) range from −18.9 and −145‰ to −16.0 and −125‰, respectively. During low-flow conditions spring water DIC $\delta^{13}C$ values ranged from −11.8‰ (China Row Spring) to −9.9‰ (Ricks Spring). The range increased during high-flow conditions, from −12.3‰ (Ricks Spring) to −8.5‰ (Spring Hollow Spring).

High-flow compositions in the springs represent a mixture of new seasonal snowmelt transported in surface water, shallow groundwater or both with preexisting groundwater. Thus, the high-flow isotope values for the snowmelt addition (Table 3) have been corrected using a simple volume-balance equation (after Kendall and Doctor 2003) that shift the high-flow $\delta^{18}O$ values to −18.3‰ to −17.4‰. The $\delta^{2}H$ and $\delta^{13}C$ value adjustments are within analytical error (<2‰ and <0.1‰, respectively).

Table 3 Oxygen and hydrogen (‰ versus VSMOW) and carbon (‰ versus VPDB) stable isotope values in springs

Spring	March 2017 $\delta^{18}O$	March 2017 $\delta^{2}H$	March 2017 $\delta^{13}C$	May 2017 $\delta^{18}O^{a}$	May 2017 $\delta^{18}O^{b}$	May 2017 $\delta^{2}H^{a}$	May 2017 $\delta^{2}H^{b}$	May 2017 $\delta^{13}C^{a}$	May 2017 $\delta^{13}C^{b}$	November 2017 $\delta^{13}C$
Ricks	−17.0	−124	−9.9	−17.4	−17.4	−127	−127	−12.3	−12.3	–
Benchmark	−17.6	−137	−10.2	−18.2	−18.3	−135	−135	−10.6	−10.5	−11.6
Logan Cave	−16.6	−129	−11.6	−17.6	−17.7	−132	−133	−11.8	−11.8	–
Woodcamp	−16.9	−132	−11.3	−17.8	−18.0	−131	−131	−8.8	−8.4	–
China Row	−16.5	−129	−11.8	−17.1	−17.9	−128	−127	−11.7	−11.9	−12.5
Dewitt	−16.9	−128	−11.0	−17.6	−17.7	−125	−124	−9.1	−8.9	−12.1
Spring Hollow	−17.0	−125	−10.0	−17.5	−17.5	−124	−124	−8.5	−8.4	−11.5

[a] Undjusted

[b] Measured values are adjusted for recent snowmelt contributions by mass balance (after Kendall and Doctor 2003)

Table 4 Locations and stable isotope values (‰ versus VSMOW) of snow cores collected at different elevations in the Bear River Range

Easting (m)	Northing (m)	$\delta^{18}O$ (‰)	$\delta^{2}H$ (‰)	Elevation (m asl)
452,983.0	4,637,132.2	−17.9	−139	1,916
451,772.1	4,637,002.1	−18.0	−141	2,076
451,175.5	4,637,043.2	−17.6	−135	2,208
451,894.7	4,636,045.2	−18.3	−140	2,000
440,376.2	4,622,543.2	−16.9	−132	1,543
446,226.5	4,627,493.1	−16.0	−125	1,650
446,341.0	4,627,372.2	−16.6	−129	1,630
450,639.3	4,631,504.2	−17.0	−131	1,795
453,289.8	4,642,435.1	−18.6	−143	2,044
455,201.9	4,646,541.2	−18.9	−145	2,208
458,440.6	4,645,404.2	−18.9	−144	2,279
459,770.4	4,642,821.1	−18.3	−141	2,351
460,723.5	4,641,518.1	−18.8	−142	2,393
461,946.3	4,641,061.2	−18.4	−139	2,310
462,316.6	4,641,808.2	−18.9	−142	2,266
464,407.3	4,641,242.1	−16.7	−126	2,023
467,051.4	4,641,714.2	−17.9	−134	1,812

Tritium and CFCs

Tritium concentrations reported in tritium units (TU) and chlorofluorocarbon-11, -12, and - 113 concentrations in picomoles per kilogram (pmol/kg) are summarized in Table 5. In order to estimate the probable equivalent atmospheric concentration of CFCs at the time of recharge in parts-per-thousand by volume (pptv), a correction factor using estimates of recharge temperature and elevation was applied (Plummer et al. 2006). Air temperature in a thick unsaturated zone is typically close to the mean annual temperature (Busenberg and Plummer 1992). In Logan Canyon, the mean annual air temperature at SNOTEL sites from multiple elevations is approximately 4.5 °C (USDA 2018). Recharge elevations were estimated from highest-elevation dye-traced source locations (Spangler 2001) for Benchmark and Dewitt Springs. China Row and Spring Hollow springs were not dye traced. Their recharge elevations were estimated from the $\delta^{18}O$-elevation gradient determined in this study, and are presented in the following section.

A local record of ^{3}H atmospheric concentrations was estimated by correlation of existing records from the Salt Lake City, Utah, station (1963–1984) with records from the Ottawa, Canada, station (1953–2012) following the linear regression procedure after Michel (1989):

$$SL = 1.2 \times OT - 9.0 \quad (2)$$

where SL is the atmospheric ^{3}H concentration (in TU) at the Salt Lake City station, and OT is the concentration (in TU) at the Ottawa station. The reconstructed tritium curve for Salt Lake City is shown in Fig. 4. All spring concentrations lie within the range of estimated atmospheric values for Salt Lake City (Table 5), and hence may be assessed via lumped-parameter models (Solder et al. 2016).

The CFC-12 concentration in China Row Spring is high enough to indicate some form of contamination (W. Mace, University of Utah Noble Gas Lab, written communication, 2018). The CFC-11 concentration in China Row Spring, if taken alone, is high enough to confound whether the recharge is contemporary or stems from the 1980s. However, the CFC-113 concentration is low enough to unambiguously attribute a pre-1990 recharge age. Values for all other springs are low enough to reasonably infer recharge ages.

Discussion

Water–rock interactions

PHREEQC water–rock reaction-path models

PHREEQC simulations of open and closed reaction paths of water with stoichiometric dolomite and calcite are explored for pCO_2 conditions from $10^{-3.4}$ to $10^{-1.5}$ (Fig. 5). Measured spring values of pH and total dissolved inorganic carbon (TDIC) and calculated SI fall on open system simulations for pCO_2 conditions between $10^{-2.5}$ and $10^{-2.0}$, consistent with

Table 5 Chlorofluorocarbon (±5%) and tritium (±1 TU) concentrations in select springs

Spring	Recharge elevation (m)	(pmol/kg)	CFC-11 (pptv)	(pmol/kg)	CFC-12 (pptv)	(pmol/kg)	CFC-113 (pptv)	Tritium (TU)
Benchmark	2,133	2.40	108.11	1.36	244.84	0.16	23.18	1.9
China Row	2,026	4.74	210.97	3.04	539.34	0.36	50.51	3.5
Dewitt	1,981	3.50	154.74	2.22	390.98	0.21	29.43	4.2
Spring Hollow	1,947	1.03	45.37	1.17	205.79	0.11	15.75	4.1

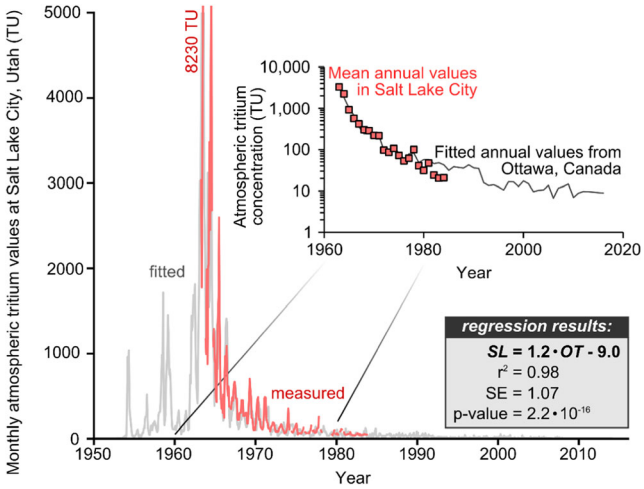

Fig. 4 Estimated time-series of atmospheric tritium concentrations (USGS GDL 2017) based on correlation with the Ottawa, Ontario IAEA station

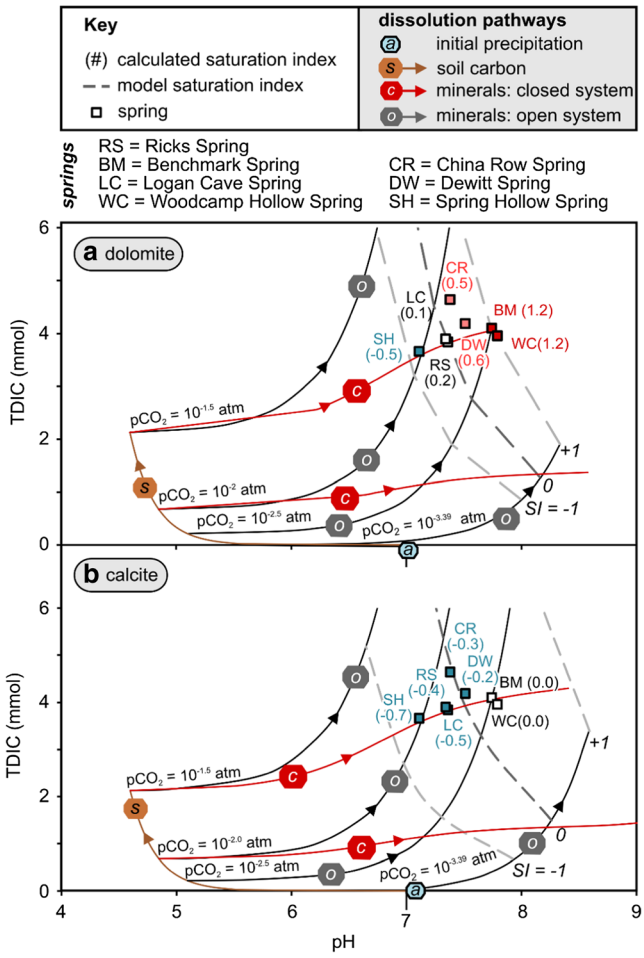

Fig. 5 **a** Reaction paths for groundwater interaction with stoichiometric dolomite along flowpaths with different fixed pCO_2 values. **b** Reaction paths for groundwater interaction with calcite along flowpaths with different fixed pCO_2 values

the pCO_2 for the spring waters (Table 2). Note that closed system reaction at a pCO_2 of approximately $10^{-1.5}$ also matches the water compositions for the dolomite and calcite scenarios; however, this pCO_2 is significantly higher than observed. Thus, these reaction-path models indicate that open-system water–rock reaction with calcite and dolomite are most likely.

Carbon stable isotope evolution models

Mass-balance calculations after Wigley (1972) were applied to test whether water–rock interactions likely occur in an open or closed system. For these calculations, the $\delta^{13}C$ values of CO_2 for precipitation in equilibrium with atmospheric CO_2 was set to the current regional average (−7.3‰; Vogel et al. 1970), the $\delta^{13}C$ for soil CO_2 was set to the average value in the proximal Wasatch Mountains (−23.3‰; Cerling et al. 1991), and the mean $\delta^{13}C$ value for the Garden City Limestone (−0.95‰; Davis 2017) was used to represent the carbonate bedrock.

Open- and closed-system water–rock reaction paths are explored in Fig. 6. The measured $\delta^{13}C$ values and TDIC concentrations best match open-system evolution at pCO_2 between $10^{-2.5}$ and $10^{-2.0}$ to equilibrium with calcite and dolomite. Closed-system paths at these pCO_2 conditions can produce $\delta^{13}C$ values similar to those observed, but at far lower TDIC concentrations. These simulations support evolution in an open system, implying that dissolution occurs mostly in conduit-dominated flowpaths that quickly transmit water. As this is the case across seasons for all observed springs, irrespective of discharge, it is likely that karst development is relatively uniform across the Bear River Range, and that flowpaths to each spring have similar hydrogeologic properties.

Congruent versus incongruent dissolution along flowpaths

The geochemical modeling presented above assumes that the aquifer materials dissolve congruently, with no coincident mineral precipitation. If so, Ca:Mg molar ratios for stoichiometric dolomite (1.0), calcian dolomite (1.1–1.3), and calcite (44–89) in the Bear River Range (Kaliser 1972) should be reflected in spring compositions from flowpaths within different geologic units. Ratios cluster around one in all springs during low-flow conditions (Table 6).

Lower water temperatures during low-flow conditions (interpreted as baseflow) indicate the possibility for incongruent dissolution, driven by increased solubility of dolomite over calcite in colder water (Williams et al. 2007). Langmuir (1971) and Wigley (1972) document the incongruent dissolution of dolomite in low-temperature water; hence, winter baseflow conditions may drive water–rock interactions to achieve Ca:Mg molar ratios of less than one.

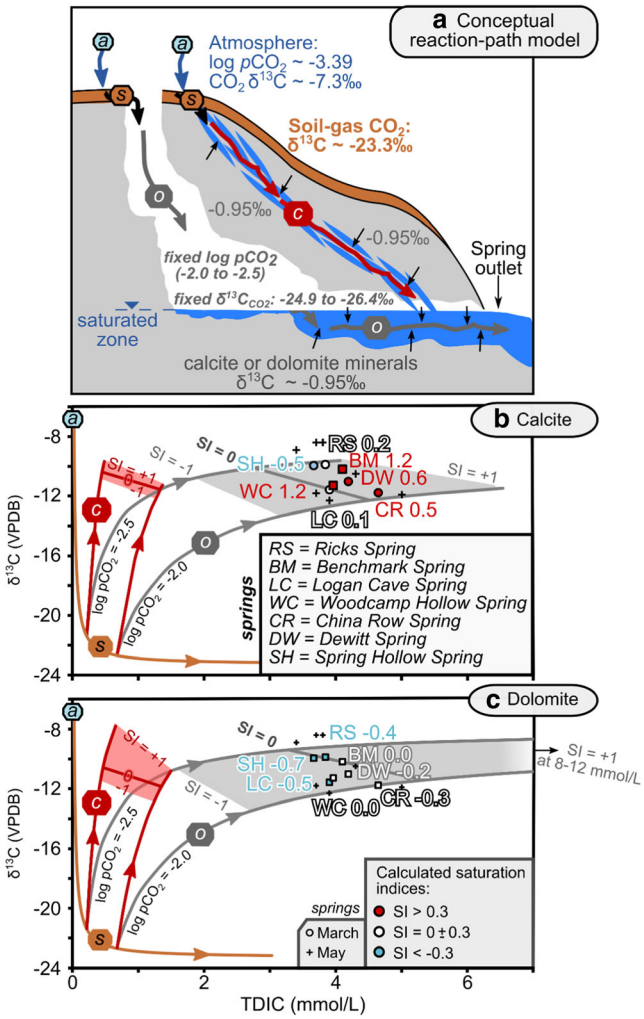

Fig. 6 **a** Conceptual $\delta^{13}C$-evolution reaction-path model. **b** $\delta^{13}C$-evolution reaction-paths for groundwater dissolution of stoichiometric calcite in open- (*O*) or closed-system (*C*) conditions. **c** $\delta^{13}C$-evolution reaction-paths for groundwater dissolution of dolomite in open- (*O*) or closed-system (*C*) conditions

To test if low Ca:Mg molar ratios reflect incongruent dissolution, PHREEQC was used to simulate dissolution of stoichiometric or calcian dolomite (Fig. 7). Thermodynamic data from Wigley (1972) were used to represent calcian dolomite in the model (Ca:Mg molar ratio = 1.17:1). The results show that dissolution will proceed incongruently after water reaches supersaturation or saturation, respectively, with stoichiometric or calcian dolomite. Reaction paths for congruent dissolution of calcian dolomite, fixed at pCO_2 values of $10^{-3.0}$ and $10^{-2.0}$ atm, respectively, explain the observed concentrations only for Spring Hollow and Ricks Springs. Similarly, reaction paths for congruent dissolution of stoichiometric dolomite at the same fixed pCO_2 values explain the observed concentrations for Benchmark, Dewitt and Logan Cave springs, and possibly China Row Spring. However, reaction paths for incongruent dissolution of calcian dolomite at these fixed pCO_2 values explain the observed concentrations for all seven springs, including Woodcamp Hollow Spring. This supports the notion that at least some incongruent dissolution occurs in the Bear River Range karst aquifer system. Hence, it is unlikely that Ca:Mg molar ratios are a reliable metric for fingerprinting particular hydrogeologic units in alpine karst.

Table 6 Ca:Mg molar ratios for springs in Logan Canyon

Spring	March T (°C)	2017 Ca:Mg	May T (°C)	2017 Ca:Mg
Ricks	5.7	1.16	8.1	1.34
Benchmark	9.6	1.04	11.0	1.04
Logan Cave	7.3	0.93	9.1	0.99
Woodcamp	7.1	0.73	9.3	0.69
China Row	7.0	0.93	7.9	0.90
Dewitt	7.5	0.97	6.4	1.59
Spring Hollow	6.4	1.18	6.7	1.97

As with the Ca:Mg molar ratios, the saturation indices may yield insight into the type of dissolution. Saturation indices for calcian or stoichiometric dolomite and magnesian calcite of the March 2017 samples are positively correlated and adhere to a linear trend (Fig. 8a). Indices from subsequent sampling excursions cluster near slight dolomite supersaturation and calcite undersaturation. Calcite saturation is never exceeded, even though dolomite saturation indices exceed a value of one. This is a hallmark of incongruence (Langmuir 1971).

All springs except Spring Hollow Spring discharge groundwater supersaturated with respect to stoichiometric dolomite (Fig. 8a), but groundwater never exceeds saturation with respect to calcian dolomite (Fig. 8b). Undersaturation with respect to stoichiometric dolomite in Spring Hollow Spring waters may stem from mixing of groundwater from two different flowpaths. This likely is the case, as Spring Hollow Spring bears a $\delta^{13}C$ value and a TDIC concentration of water supersaturated with respect to dolomite (Fig. 6).

Dissolution of calcian dolomite inherently produces one degree of supersaturation with respect to stoichiometric dolomite, removing the need for additional mechanisms. All springs adhere closely to the simulated reaction path of dissolving calcian dolomite, and never reach supersaturation with respect to it or calcite (Fig. 8b). Hence, it is likely that incongruent dissolution of calcian dolomite, where present, exerts a strong control on water–rock interactions.

Oxygen and hydrogen stable isotopes

Meteoric water isotopic characteristics

The $\delta^{18}O$ and $\delta^{2}H$ values for spring waters are similar to those for precipitation in Utah (Fig. 9; Bowen 2017). Most spring samples collected in March appear to fall below (to the right

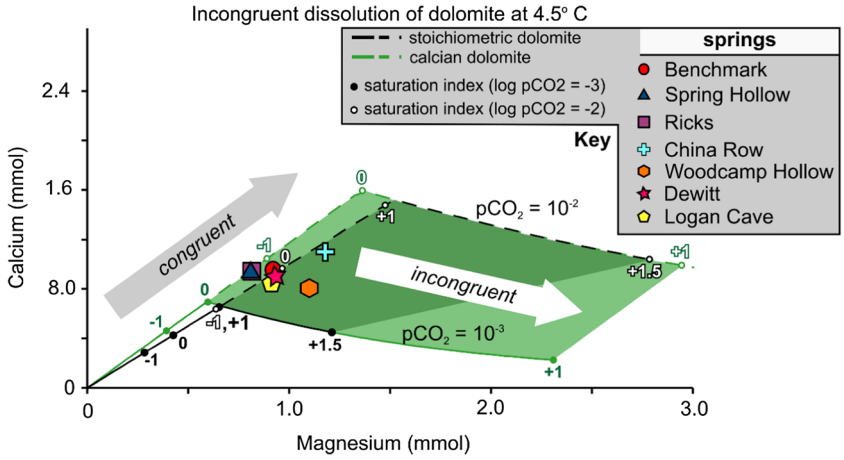

Fig. 7 Calcium and magnesium mass evolution via incongruent dissolution of stoichiometric or calcian dolomite and measured values in Bear River Range springs

of) the global and local meteoric water lines (Craig 1961; Kendall and Coplen 2001). Snow samples lie along a significant linear trend (shown in blue on Fig. 9) with a slope similar to the Utah meteoric water line (Kendall and Coplen 2001) and given by the formula:

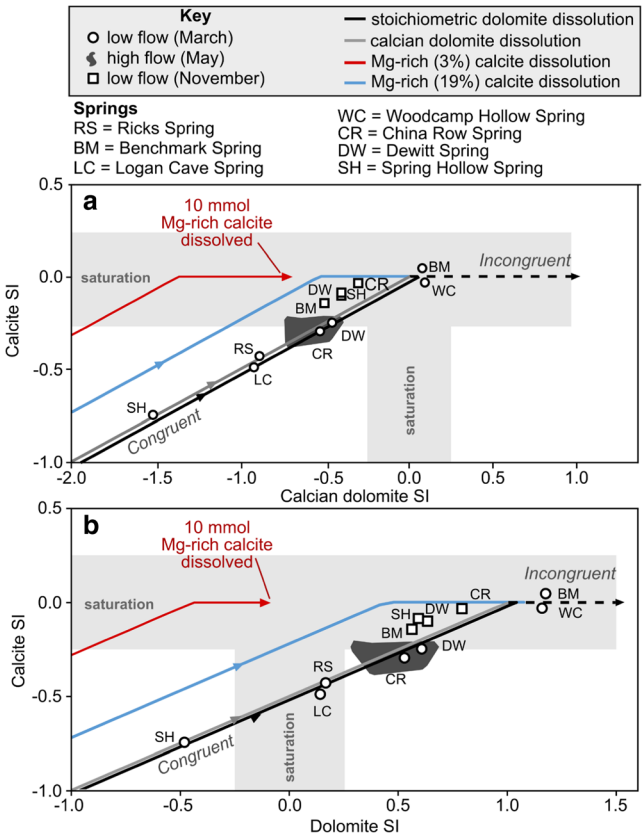

Fig. 8 **a** Modeled saturation indices for dissolution of stoichiometric or calcian dolomite and magnesian calcite, along with calculated values for Bear River Range springs, shown in terms of saturation with respect to calcite and dolomite. **b** Modeled saturation indices for dissolution of stoichiometric or calcian dolomite and magnesian calcite, along with calculated values for Bear River Range springs, shown in terms of saturation with respect to calcite and calcian dolomite

$$\delta^2H = 6.6 \times \delta^{18}O + 13.3 \quad (3)$$

On average, the spring isotope values measured in May are lower than those during March. This may reflect a seasonal difference where May conditions include winter precipitation in the form of snowmelt recharge and March reflects the isotopic value of late-fall recharge or a longer-term mean groundwater value. However, it seems unlikely that this represents an evaporative trend because all of the values lie within the range of observed values for precipitation in Utah (Bowen 2017). The range of snow isotope values encompasses the values measured in spring water, but also include much lower values. The lower values recorded by the snow is consistent with winter precipitation (Earman et al. 2006; Sharp 2007).

Stable-isotope elevation gradients

Oxygen stable isotope ratios for snow at different elevations are reported in Table 4. The $\delta^{18}O$ values were assessed by analysis-of-variance (ANOVA) to correlate statistically the dominant geographic controls on fractionation. This tests the hypothesis proposed by Bright (2009) that progressive rainout (or precipitation as snow) of air masses traversing the Bear River Range is more significant than elevation on the $\delta^{18}O$ values of precipitation. ANOVA ranks the significance of possible controlling factors (e.g., longitude and elevation), and informs the choice of variables for subsequent linear regression (Berthoux and Brown 2002).

The results (Table 7) suggest that elevation is the primary influence on fractionation in the Bear River Range. Although the F-statistic indicates a possible effect of longitude on $\delta^{18}O$ values, iterative adjustment shows that it is not significant in conjunction with elevation, and decreases in significance when assessed separately. Elevation increases in significance to greater than 99.9% when used as the only predictor, which is evidence for a better empirical link. Hence, elevation (m asl) was chosen as the sole predictor variable for $\delta^{18}O$ values in linear regression:

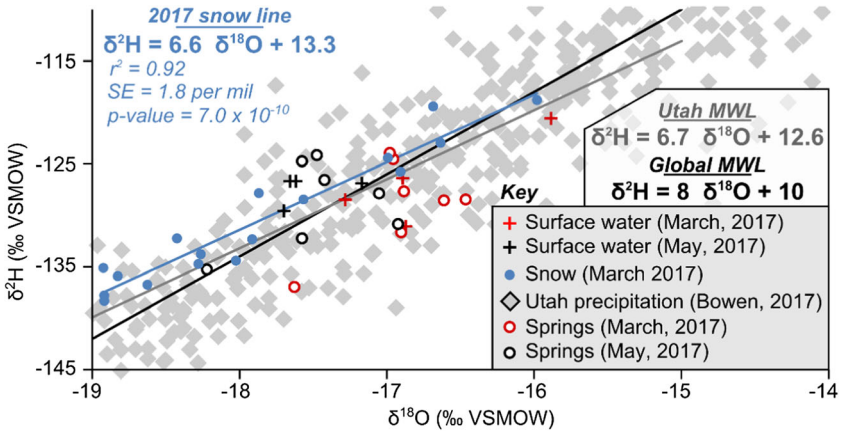

Fig. 9 Oxygen and hydrogen isotopes for springs, streams, and snow in the Bear River Range in comparison to the global (Craig 1961) and Utah (Kendall and Coplen 2001) meteoric water lines (MWL)

$$\delta^{18}O = -0.0028 \times \text{Elevation} - 12.2 \quad (4)$$

The elevation isotope gradient (line slope) is −0.28‰ per 100 m. This gradient is similar to others for rain in the United States, but contradicts other interpretations that such gradients do not exist in snow or away from coasts (Abbott et al. 2000; James et al. 2000; Blasch and Bryson 2007; Brooks et al. 2012).

Groundwater recharge elevations often are estimated from elevation-gradient regression of $\delta^{18}O$ snow values (James et al. 2000; Poage and Chamberlain 2001). Mean recharge elevations estimated from the linear relationship with $\delta^{18}O$ values are summarized in Table 8. The $\delta^{18}O$-predicted mean recharge elevations qualitatively align with dye-trace estimates, except for Ricks and Benchmark springs. The mean $\delta^{18}O$-predicted recharge elevation for Ricks Spring is lower than the two far higher dye-traced sources (Fig. 2), Tony Grove (640 m) and Bunchgrass Hollow (805 m). The $\delta^{18}O$ value for Ricks Spring (−17.4‰; Table 8) likely represents mixing of high-elevation recharge with a significant amount of Logan River water ($\delta^{18}O = -17.6$‰; Spangler 2001). In contrast, the $\delta^{18}O$-predicted mean recharge elevation for Benchmark Spring is higher than the dye-trace estimate (Table 8). Because Benchmark Spring's stable-isotope signature is consistently more negative than Logan Cave Spring's (Table 3), it is likely that the former's recharge area is higher than the latter's dye-traced source, despite dye traces that link both springs to a shared surface catchment (Fig. 2).

Groundwater residence times

Groundwater age estimates from lumped-parameter models (LPMs) of ^{3}H and CFC data are presented in this section. Chlorofluorocarbon concentrations in pmol/kg were corrected for temperature and recharge elevation, then converted to atmospheric units of pptv after Busenberg et al. (2006). The corrected values are less than contemporary atmospheric concentrations except for CFC-12 in China Row Spring, which is likely contaminated (W. Mace, University of Utah Noble Gas Lab, written communication, 2018). Accordingly, China Row Spring was excluded from LPMs that involved CFC-12.

Binary-mixing model

Dye traces document the ability of some baseflow to move through Bear River Range karst with subannual transit times (Spangler 2002). This suggests that a binary-mixing model fixed at modern concentrations may be more accurate than a simple piston-flow model of older water.

The applicable age range for a binary-mixing model is limited to the date that each tracer was first detected in the atmosphere. The earliest detection at Niwot Ridge occurred in 1940 for CFC-11 and CFC-12, and in 1943 for CFC-113 (Jurgens et al. 2012). Earliest detection of tritium above background levels occurred in 1945 at the Ottawa, Ontario station. Hence, age estimates by this method are only possible if groundwater is younger than 75–80 years.

Binary mixing models of ^{3}H and each CFC support the notion that groundwater is a mixture of subannual and decadal

Table 7 Significance of longitude and elevation to $\delta^{18}O$ in the analysis of variance

Factors	Variable	Degrees of freedom	Sum of squares	F-statistic	Significance
Two factors	Longitude	1	3.8	10	>99%
	Elevation	1	5.3	14	>99%
One factor	Elevation	1	9	26	>99%

Table 8 Mean elevations and 95% confidence intervals for the snowpack contributing recharge to springs in Logan Canyon, estimated from the elevation gradient

Spring	$\delta^{18}O$ (‰) (adjusted)	Mean recharge elevation above outlet (m asl)	95% confidence interval (m)	Dye-traced elevation range above outlet (m asl) (Spangler 2001)
Ricks	−17.4	134	±97	73–805
Benchmark	−18.3	371	±97	98–122
Logan Cave	−17.7	293	±88	37–390
Woodcamp	−18.0	422	±87	335–963
China Row	−17.9	406	±87	–
Dewitt	−17.7	445	±89	390–878
Spring Hollow	−17.5	326	±93	–

recharge, in this case 60–65 years old (Fig. 10; Table 9). The estimated percentages of decadal recharge present in baseflow using ^{3}H (0–80% decadal) vary more than those predicted using CFCs (40–85% decadal).

It is likely that zones of lesser karstification exist in each spring's groundwater basin, yet only inhibit flow by several decades; however, the results of the binary-mixing model do not rule out the possibility that a small percentage of much older (centennial to millennial) recharge may be mixing with subannual and decadal recharge.

Residence time of this magnitude was documented using ^{3}H concentrations in dripwater recharge to a cave system in Israel (Even et al. 1986). The spread for the decadal-age component is similar to that of probability-density functions (PDFs) of age simulated for a karst aquifer in South Dakota (Long and Putnam 2009). If this is the case, extended droughts could significantly affect the baseflow of critical water resources decades later. Furthermore, the possible absence of matrix-dominated flow in alpine karst indicates that groundwater resources would be highly responsive to long-term climate shifts.

Table 9 Groundwater age in the Bear River Range alpine-karst aquifer system according to a binary-mixing model of chlorofluorocarbon and tritium concentrations

Spring	Tracers	% of discharge	Age (years)
Dewitt	CFC-11 and ^{3}H	30%	60
	CFC-12 and ^{3}H	25%	60
	CFC-113 and ^{3}H	45–70%	60
Spring Hollow	CFC-11 and ^{3}H	80%	60
	CFC-12 and ^{3}H	60%	60
	CFC-113 and ^{3}H	75%	60
Benchmark	CFC-11 and ^{3}H	50%	65
	CFC-12 and ^{3}H	55%	65
	CFC-113 and ^{3}H	65%	65
China Row	CFC-11 and ^{3}H	0–10%	60
	CFC-113 and ^{3}H	25%	60

Conclusions

Observed spring $\delta^{13}C$ DIC values range from −11.8 to −9.9‰, which are intermediate between carbonate bedrock (~ −1‰) and local soil CO_2 (~ −23‰). Modeled reaction paths for dissolution in an open system align well with data presented in this study. Saturation indices and low Ca:Mg molar ratios indicate that incongruent dissolution exerts a strong control on water–rock interactions. Reaction path modeling indicates that dissolution of calcian dolomite (Ca:Mg molar ratio = 1.17:1), a primary aquifer material in the Bear River Range, exerts strong control on water geochemistry. These results support Bright's (2009) conclusion that incongruent dissolution of calcian dolomite controls groundwater chemistry in the Bear River Range, and contrast with previous inferences of a less solution-enhanced, matrix-dominated flowpath that would be more resilient to climate change (Kolesar et al. 2005; Neilson et al. 2018).

Spring water $\delta^{18}O$ and $\delta^{2}H$ values are similar to Utah meteoric water. The $\delta^{18}O$ values in the alpine snowpack display a significant statistical relationship with elevation (−0.28‰ per 100 m), suggesting that it may be a useful tracer for groundwater recharge elevation. Predicted recharge elevations from the $\delta^{18}O$ gradient qualitatively align with dye-trace estimates. However, Ricks and Benchmark Springs have $\delta^{18}O$ values that do not align well with dye-traced recharge elevations. It is likely that Ricks Spring represents a mix of alpine snowmelt and Logan River water. If Benchmark Spring, like Logan Cave Spring nearby, draws recharge from higher elevations, both should have similar isotopic values from snowmelt runoff during high-flow conditions. Benchmark Spring's stable-isotope signature is clearly more negative across seasons (Table 3); hence, it is likely that a higher recharge zone supplies water to Benchmark Spring.

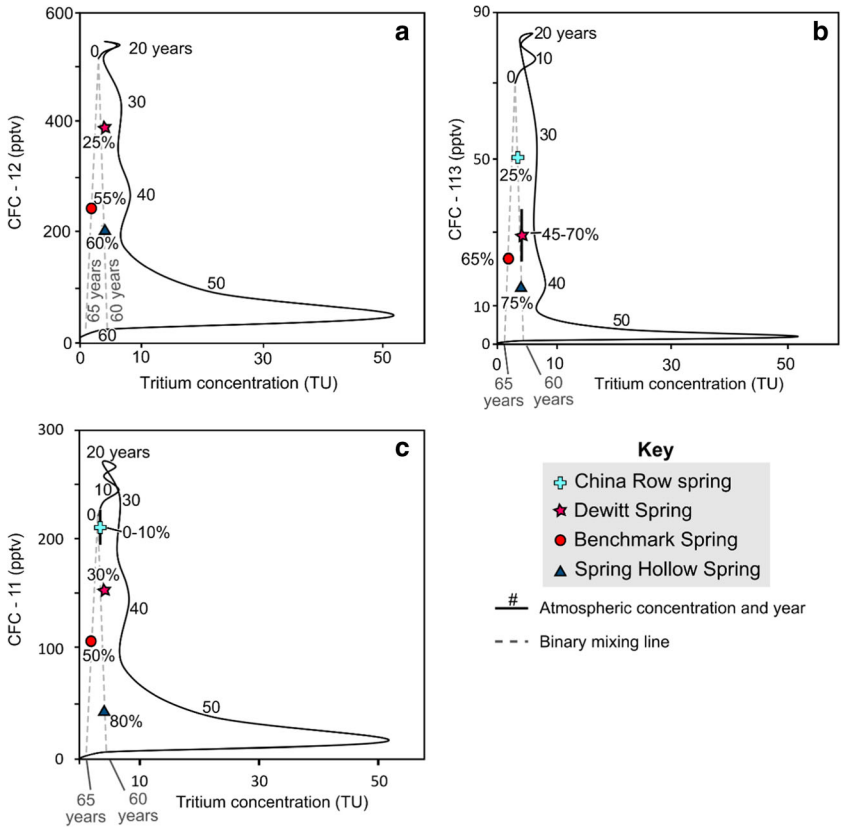

Fig. 10 Tritium and chlorofluorocarbon binary-mixing models of groundwater age in the Bear River Range alpine-karst aquifer system: **a** CFC-12, **b** CFC-113, **c** CFC-11. Dashed lines connect subannual recharge ages with decadal ages ranging from 60 to 65 years

Tritium and chlorofluorocarbon concentrations in representative springs are likely best described by binary mixing of subannual recharge with 60- to 65-year-old groundwater. This suggests that the alpine karst aquifer system in the Bear River Range is best represented by a double-porosity, rather than a triple-porosity, model (Fig. 3b). The subannual recharge documented by dye traces implies that caverns are the primary flowpath to each spring, but the possible presence of decadal-age water may indicate that a slightly lower permeability flowpath dominates during baseflow. Nonetheless, the binary-mixing model results do not rule out the possibility that a relatively small proportion of matrix flow occurs, and that a triple-porosity system exists.

Neilson et al. (2018) concluded that matrix-dominated flow plays a role in the karst hydrology of the Bear River Range; however, the results of the present investigation suggest that such a role is negligible. The documented subannual recharge indicates the importance of conduit flow. This combined with the strong likelihood that open-system conditions dominate supports the conclusion that the alpine karst aquifer system can be described best by a double-porosity model. If this is indeed the case, the aquifer system may not provide drought resilience for water resources linked to it. Further study of this aquifer system, as well as other alpine karst systems in arid to semiarid settings, with an enhanced suite of geochemical tracers, including carbon-14 and helium-3, will help refine the understanding of potential matrix-dominated flow, and improve management of alpine-karst water resources in light of climate change.

Acknowledgements The authors thank reviewers Brad Esser and Stephane Binet, as well as associate editor Hervé Jourde and editor Prof. Rui Ma, whose insights and suggestions greatly improved the final version of this work.

References

Abbott MD, Lini A, Bierman PR (2000) $\delta^{18}O$, δD, and ^{3}H measurements constrain groundwater recharge patterns in an upland fractured bedrock aquifer, Vermont, USA. J Hydrol 228:101–112

Bahr K (2016) Structural and lithological influences on the Tony Grove alpine karst system, Bear River range, north-central Utah. MSc Thesis, Utah State University, Logan, UT, 212 pp

Berthoux PM, Brown LC (2002) Statistics for environmental engineers. CRC, Boca Raton, FL, 512 pp

Bischoff WD (1998) Dissolution enthalpies of magnesian calcites. Aquat Geochem 4:321–336

Bjorklund LJ, McGreevy LJ (1971) Groundwater resources of Cache Valley, Utah and Idaho. Technical Publication 36, Utah Department of Natural Resources, Salt Lake City, 72 pp

Blasch KW, Bryson JR (2007) Distinguishing sources of ground water recharge by using $\delta^{2}H$ and $\delta^{18}O$. Ground Water 45(3):294–308

Bowen G (2017) water isotopes database. http://waterisotopes.org. Accessed October 2018

Bright J (2009) Isotope and major-ion chemistry of groundwater in bear Lake Valley, Utah and Idaho, with emphasis on the Bear River range. In: Rosenbaum JG, Kaufman DS (eds) Paleoenvironments

of Bear Lake, Utah and Idaho, and its catchment. Geol Soc Am Spec Pap 450:105–132

Brooks JR, Wiginton PJ, Phillips DL, Comeleo R, Coulombe R (2012) Willamette River basin surface water isoscape ($\delta^{18}O$ and $\delta\ ^{2}H$): temporal changes of source water within the river. Ecosphere 3(5): 1–39

Busenberg E, Plummer LN (1992) Use of chlorofluorocarbons (CCl_3F and CCL_2F_2) as hydrologic tracers and age-dating tools: the alluvium and terrace system of central Oklahoma. Water Resour Res 28(9):2257–2283

Busenberg E, Plummer LN, Cook PG, Solomon DK, Han LF, Groning M, Oster H (2006) Sampling and analytical methods. In: Use of chlorofluorocarbons in hydrology: a guidebook. International Atomic Energy Agency, Vienna, pp 199–220

Cerling TE, Solomon DK, Quade JA, Bowman JR (1991) On the isotopic composition of carbon in soil carbon dioxide. Geochim Cosmochim Acta 55:3403–3405

Chen Z, Goldscheider N (2014) Modeling spatially and temporally varied hydraulic behavior of a folded karst system with dominant conduit drainage at catchment scale, Hochifen-Gottesacker, Alps. J Hydrol 514:41–52

Craig H (1961) Isotopic variations in meteoric waters. Science 133(3465):1702–1703

Davis CR (2017) Sequence stratigraphy, chemostratigraphy, and biostratigraphy of lower Ordovician units in northeastern and western Central Utah: regional implications. MSc Thesis, Utah State University, Logan, UT, 244 pp

Dover JH (1995) Geologic map of the Logan 30′ × 60′ quadrangle, Cache and Rich counties, Utah, and Lincoln and Uinta counties, Wyoming 1:100,000. Utah Geological Survey Miscell Publ MP06–8 DM, Utah Geological Survey, Salt Lake City, UT

Earman S, Campbell AR, Phillips FM, Newman BD (2006) Isotopic exchange between snow and atmospheric water vapor: estimation of the snowmelt component of groundwater recharge in the southwestern united state. J Geophys Res 111:1–18

Evans JP, Oaks RQ Jr (1996) Three-dimensional variations in extensional fault shape and basin form: the Cache Valley basin, eastern basin and range province, United States. Geol Soc Am Bull 108:1580–1593

Evans JP, McCalpin JP, Holmes DC (1996) Geologic map of the Logan quadrangle, Cache County, Utah 1:24,000. Utah Geological Survey Map 96–1, Utah Geological Survey, Salt Lake City, UT

Even H, Carmi I, Magaritz M, Gerson R (1986) Timing the transport of water through the upper vadose zone in a karstic system above a cave in Israel. Earth Surf Process Landf 11(2):181–191

Filippini M, Squarzoni G, De Waele J, Fiorucci A, Vigna B, Grillo B, Riva A, Rossetti S, Zini L, Casagrande G, Stumpp C, Gargini A (2018) Differentiated spring behavior under changing hydrological conditions in an alpine karst aquifer. J Hydrol 556:572–584

Ford DC (1983) Effects of glaciations upon karst aquifers in Canada. J Hydrol 61:149–158

Ford D, Williams PD (2007) Karst hydrogeology and geomorphology. Wiley, West Sussex, England, 576 pp

Francis GG (1972) Stratigraphy and environmental analysis of the swan peak formation and Eureka quartzite, northern Utah. MSc Thesis, Utah State University, Logan, UT, 125 pp

Frondini F, Zucchini A, Comodi P (2014) Water–rock interactions and trace element distribution in dolomite aquifers: the Sassolungo and Sella systems (northern Italy). Geochem J 48:231–246

Goldscheider N, Neukum C (2010) Fold and fault control on the drainage pattern of a double-karst-aquifer system, Winterstaude, Austrian Alps. Acta Carsol 39(2):173–186

Gooseff MN, Evans JP, Kolesar P, Lachmar TE, Payn R (2005) Hydrologic contributions of springs to the Logan River, Utah. Abstract H51C-02, AGU Spring Meeting, New Orleans, LA, May 2005

Gremaud V, Goldscheider N, Savoy L, Favre S, Masson H (2009) Geological structure, recharge processes and underground drainage of a glacierised karst aquifer system, Tsanfleuron-Sanetsch, Swiss Alps. Hydrogeol J 17:1833–1848

International Atomic Energy Agency (IAEA) (2014) Global network of isotopes in precipitation, the GNIP database. http://www.iaes.org/water. Accessed August 2017

James ER, Manga M, Rose TP, Hudston GB (2000) The use of temperature and the isotopes of O, H, C, and noble gases to determine the pattern and spatial extent of groundwater flow. J Hydrol 237:100–112

Jurgens BC, Bohlke JK, Eberts SM (2012) TracerLPM (version 1): an Excel® workbook for interpreting groundwater age distributions from environmental tracer data. US Geol Surv Tech Methods Rep 4-F3, 60 pp

Kaliser BN (1972) Environmental geology of Bear Lake area, Rich County, Utah. Utah Geol Mineral Surv Bull 96, 32 pp

Katz BG, Sepulveda AA, Verdi RJ (2009) Estimating nitrogen loading to ground water and assessing vulnerability to nitrate contamination in a large karstic springs basin, Florida. J Am Water Resour Assoc 45(3):607–627

Kendall C, Coplen TB (2001) Distribution of oxygen-18 and deuterium in river waters across the United States. Hydrol Process 15:1363–1393

Kendall C, Doctor DH (2003) Stable isotope applications in hydrologic studies. In: Drever J (ed) Treatise on geochemistry, vol 5. Elsevier, Amsterdam, The Netherlands, pp 319–364

Kolesar PT, Evans JP, Gooseff MN, Lachmar TE, Payn R (2005) A tale of two (or more) karsts, Bear River Range, Cache National Forest. Utah Geol Soc Am Abstr Programs 37(7):177

Langmuir D (1971) Geochemistry of some carbonate ground waters in central Pennsylvania. Geochim Cosmochim Acta 35(10):1023–1045

Lauber U, Goldscheider N (2014) Use of artificial and natural tracers to assess groundwater transit-time distribution and flow systems in a high-alpine karst system (Wetterstein Mountains, Germany). Hydrogeol J 22:1807–1824

Long AJ, Putnam LD (2009) Age-distribution estimation for karst groundwater: issues of parameterization and complexity in inverse modeling by convolution. J Hydrol 376:579–588

McCalpin JP (1989) Surficial geologic map of the East Cache fault zone, Cache County, Utah 1:50,000. US Geol Surv Miscell Field Studies Map MF-2107

McCalpin JP (1994) Neotectonic deformation along the east cache fault zone, Cache County, Utah. Utah Geol Surv Spec Study 83, 37 pp

Michel RL (1989) Tritium deposition in the continental United States, 1953-83. US Geol Surv Water Resour Invest Rep 89-4072, 46 pp

Mook W (2001) Environmental isotopes in the hydrological: introduction—theory, methods, review. Tech Doc Hydrol vol 1, 39. UNESCO/Int Atomic Energy Agency, Paris, 164 pp

Moral F, Cruz-Sanjulian JJ, Olias M (2008) Geochemical evolution of groundwater in the carbonate aquifers of Sierra de Segura (Betic Cordillera, southern Spain). J Hydrol 360:281–296

Mundorff JC (1971) Nonthermal springs of Utah. Utah Geol Mineral Surv Water Resour Bull 16, 70 pp

Neilson BT, Tennant H, Stout TL, Miller MP, Gabor RS, Jameel Y, Millington M, Gelderloow A, Bowen GJ, Brooks PD (2018) Stream centric methods for determining groundwater contributions in karst mountain watersheds. Water Resour Res 54(9):6708–6724

Niwot Ridge LTER (2018) Niwot Ridge LTER long-term ecological research dataset. http://niwot.colorado.edu/data. Accessed January 2018

Ozyurt NN (2008) Residence time distribution in the Kirkgoz karst springs (Anntalya-Turkey) as a tool for contamination vulnerability assessment. Environ Geol 53:1571–1583

Parkhurst DL, Appelo CA (2013) Description of input and examples for PHREEQC version 3: a computer program for speciation, batch-reaction, one-dimensional transport, and inverse geochemical calculations. US Geol Surv Tech Methods, Book 6, chapter A43, US Geological Survey, Reston, VA, 497 pp

Plummer LN, Busenberg E, Cook PG (2006) Principles of chlorofluorocarbon dating. In: Groning M, Han LF, Aggarwal P (eds) Use of chlorofluorocarbons in hydrology: a guidebook. International Atomic Energy Agency, Vienna, pp 17–29

Poage MA, Chamberlain CP (2001) Empirical relationships between elevation and the stable isotope composition of precipitation and surface waters: considerations for studies of paleoelevation change. Am J Sci 301:1–15

Robinson JM (1999) Chemical and hydrostratigraphic characterization of ground water and surface water interaction in Cache Valley, Utah. MSc Thesis, Utah State University, Logan, UT, 184 pp

Savio D, Stadler P, Reischer GH, Demeter K, Linke RB, Blaschke AP, Mach RL, Kirschner AKT, Stadler H, Farnleitner AH (2019) Spring water of an alpine karst aquifer is dominated by a taxonomically stable but discharge-responsive bacterial community. Frontiers Microbiol. https://doi.org/10.3389/fmicb.2019.00028

Sharp Z (2007) Stable sotope geochemistry. Pearson prentice hall. Upper Saddle River, New Jersey, p 344

Solder JE, Stolp BJ, Heilweil VM, Susong DD (2016) Characterization of mean transit time at large springs in the upper Colorado River basin, USA: a tool for assessing groundwater discharge variability. Hydrogeol J 24(8):2017–2033

Solomon DK (2017) University of Utah dissolved and noble gas lab tritium collection guide. http://www.noblegaslab.utah.edu/pdfs/tritium_collection.pdf. Accessed May 2017

Smart CC (1983) The hydrology of the Castleguard Karst, Columbia Icefields, Alberta, Canada. Arct Alp Res 15(4):471–486

Smart CC (1988) Artificial tracer techniques for the determination of the structure of conduit aquifers. Ground Water 26(4):445–453

Spangler LE (2001) Delineation of recharge areas for karst springs in Logan canyon, Bear River Range, northern Utah. US Geol Surv Water Resour Invest Rep 01-4011:186–193

Spangler LE (2002) Use of dye tracing to determine conduit flow paths within source-protection areas of a karst spring and wells in the Bear River Range, northern Utah. US Geol Surv Water Resour Invest Rep 2-4174. 6 pp

Spangler LE (2012) Karst hydrogeology of the Bear River Range in the vicinity of Logan canyon, northern Utah, Uinta-Wasatch-Cache National Forest. Beneath For 5(1):12–20

USDA (2018) Snow telemetry (SNOTEL) and snow course data and products. US Department of Agriculture, Natural Resources Conservation Service. https://www.wcc.nrcs.usda.gov/snow/. Accessed January 2018

USGS GDL (2017) Tracer input functions. US Geological Survey Groundwater Dating Laboratory, Reston, VA. http://water.usgs.gov/lab/software/air_curve/. Accessed November 2017

Vogel JC, Grootes PM, Mook WG (1970) Isotopic fractionation between gaseous and dissolved carbon dioxide. Zeitschrift Physik 230(3):225–238

White WB (2003) Conceptual models for karstic aquifers. Speleogenesis Evol Karst Aquifers 1(1):11–16

Wigley TM (1972) The incongruent solution of dolomite. Geochim Cosmochim Acta 37:1397–1402

Wilde FD (2008) Guidelines for field-measured water-quality properties (ver. 2.0). US Geological Survey Techniques of Water-Resources Investigations, book 9, chapter A6, section 6.0, USGS, Reston, VA, pp 3–29

Williams EL, Szramek KJ, Jin L, Ku TC, Walter LM (2007) The carbonate system geochemistry of shallow groundwater-surface water systems in temperate glaciated watersheds (Michigan, USA): significance of open-system dolomite weathering. Geol Soc Am Bull 119(516):515–528

Williams JS (1948) Geology of the Paleozoic rocks, Logan quadrangle, Utah. Geol Soc Am Bull 59:1121–1184

Williams JS (1958) Geologic atlas of Utah, Cache County Utah Geol Mineral Survey Bull 64, 98 pp

Zeng C, Gremaud V, Zeng H, Liu Z, Goldscheider N (2012) Temperature-driven meltwater production and hydrochemical variations at a glaciated alpine karst aquifer: implication for the atmospheric CO_2 sink under global warming. Environ Earth Sci 65:2285–2297